JACS
JOURNAL OF THE AMERICAN CHEMICAL SOCIETY

Article

pubs.acs.org/JACS

# Temperature-Enhanced Association of Proteins Due to Electrostatic Interaction: A Coarse-Grained Simulation of Actin−Myosin Binding

Kei-ichi Okazaki, Takato Sato, and Mitsunori Takano*

Department of Pure and Applied Physics, Waseda University, 3-4-1 Okubo, Shinjuku-Ku, Tokyo, Japan

**ABSTRACT:** Association of protein molecules constitutes the basis for the interaction network in a cell. Despite its fundamental importance, the thermodynamic aspect of protein−protein binding, particularly the issues relating to the entropy change upon binding, remains elusive. The binding of actin and myosin, which are vital proteins in motility, is a typical example, in which two different binding mechanisms have been argued: the binding affinity increases with increasing temperature and with decreasing salt-concentration, indicating the *entropy*-driven binding and the *enthalpy*-driven binding, respectively. How can these thermodynamically different binding mechanisms coexist? To address this question, which is of general importance in understanding protein−protein bindings, we conducted an *in silico* titration of the actin−myosin system by molecular dynamics simulation using a residue-level coarse-grained model, with particular focus on the role of the electrostatic interaction. We found a good agreement between *in silico* and in vitro experiments on the salt-concentration dependence and the temperature dependence of the binding affinity. We then figured out how the two binding mechanisms can coexist: the enthalpy (due to electrostatic interaction between actin and myosin) provides the basal binding affinity, and the entropy (due to the orientational disorder of water molecules) enhances it at higher temperatures. In addition, we analyzed the actin−myosin complex structures observed during the simulation and obtained a variety of weak-binding complex structures, among which were found an unusual binding mode suggested by an earlier experiment and precursor structures of the strong-binding complex proposed by electron microscopy. These results collectively indicate the potential capability of a residue-level coarse-grained model to simulate the association−dissociation dynamics (particularly for transient weak-bindings) exhibited by larger and more complicated systems, as in a cell.

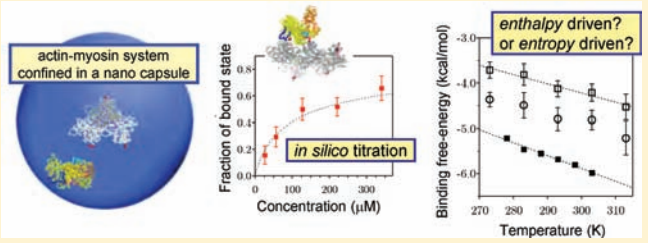


## INTRODUCTION

Cells are filled with proteins and other macromolecules that are surrounded by small chemical species such as waters, ligands, and ions. The interaction network among these macromolecules gives rise to all sorts of biological functions. Although the interaction network is desperately complicated,[1] it is worthwhile to remember that the network is based on the association reaction of two molecules (i.e., bimolecular binding). Therefore, physical understanding of the bimolecular binding, including its statistical thermodynamic aspect,[2] should become increasingly important as the studies on cell biology proceed. However, the statistical thermodynamic aspect of bimolecular binding is far from trivial, as represented by the long-standing argument about the entropy change upon binding which is inseparably related to the hydrophobic effect.[3−12] Intuitively, binding is accompanied by negative (unfavorable) entropy change due to the loss of the freedom of one molecule, but the negative (favorable) enthalpy change can overcome the unfavorable entropy change and drive the binding (i.e., the *enthalpy*-driven binding). In a vacuum, this intuition is correct although the unfavorable entropy change is largely compensated by the newly created internal motions in the complex.[2,5,7−9] In an aqueous environment, the unfavorable entropy change can be further compensated to the extent where the entropy change becomes positive, leading to the *entropy*-driven binding. While it is obvious that the overcompensation is caused by solvents,[3−5] the underlying physical mechanism is rather elusive and yet "unsolved"[10] even though considerable advances have been made[13] including recent molecular theories of the hydrophobic effect.[10−12]

Biologically important associations of proteins often appear *entropy* driven. A typical example is the association of actin and myosin, which constitute the molecular motor "actomyosin" that converts the chemical energy of ATP into mechanical force to be utilized for muscle contraction and other vital cellular functions such as vesicle trafficking, cytoplasmic streaming, and cytokinesis.[1] The actin−myosin binding is strengthened as temperature is increased,[14,15] suggesting the entropy-driven mechanism due to the hydrophobic interaction between nonpolar amino acid residues.[16] However, the binding is also strengthened as the ionic concentration of solution is lowered,[14,15] suggesting the *enthalpy*-driven mechanism due to the electrostatic interaction between charged residues. It is therefore natural that a controversy arises between the entropy- and the enthalpy-driven binding mechanisms.[17] Resolving this controversy is highly important because it should contribute not only to establishing the physical picture of the force-

**Received:** February 13, 2012
**Published:** May 4, 2012

   dx.doi.org/10.1021/ja301447j | *J. Am. Chem. Soc.* 2012, 134, 8918−8925

generation mechanism of actomyosin but also to advancing our general understanding of bimolecular association. Here we address this issue by employing an *in silico* approach as in the previous work where, by a molecular dynamics simulation using a residue-level coarse-grained model, we demonstrated the electrostatically-driven binding between actin and myosin, which leads to force-generation.[18] In the present study, we conduct a systematic *in silico* titration and show that the actin−myosin weak-binding is *enthalpy*-driven and yet is strengthened as temperature increases; i.e. the binding harnesses both the enthalpy- and entropy-driven mechanisms due to the electrostatic interaction.

Residue-level coarse-grained models have a potential to quantitatively reproduce protein−protein bindings, particularly transient weak-bindings.[19,20] However, coarse-graining of the intermolecular interaction is not straightforward, which is especially true of the hydrophobic interaction. On the other hand, the electrostatic interaction is inherently compatible with coarse-graining; in fact, the continuum model (or the dielectric model) has long been applied to protein systems. The Debye−Hückel model is one such model and has been utilized in the residue-level coarse-grained model.[18−22] We thus focus in this study on the role of the electrostatic interaction, employing the Debye−Hückel model. We show how well the residue-level coarse-grained model with the Debye−Hückel electrostatics in which temperature dependence of the dielectric constant are properly taken into account can describe the protein−protein interaction, taking the actin−myosin system as a good example where a large amount of thermodynamic and structural data has been accumulated.

## RESULTS

***In Silico* Titration of Actin−Myosin Binding.** In our *in silico* titration, actin and myosin were encapsulated in a sphere as shown in Figure 1A. In the spherical capsule, reversible binding between myosin and actin was observed many times, which is manifested in the time course of the actin−myosin interaction energy (Figure 1B). The distribution of the interaction energy, shown in Figure 1C, was clearly bimodal, with a broad peak centered around −5 kcal/mol and a sharp peak at zero, corresponding to the bound and the unbound states, respectively. This bimodal shape allowed us to set a boundary between the two states (in this study, we set the boundary at −1.2 kcal/mol) and enabled us to calculate the fractional ratio of the bound state ($f_B$). Then titration was realized by changing the radius of the sphere and accordingly by changing the concentration of myosin and actin. Thus, we were able to obtain the titration curve as shown in Figure 1D.

**Salt-Concentration Dependence of Actin−Myosin Binding.** We then conducted the titration experiment at different salt concentrations. The resulting titration curves shown in Figure 2A demonstrate that the actin−myosin binding affinity is weakened as the salt concentration is increased. The normalized (i.e., per actin monomer) dissociation constants, $\tilde{K}_d$, obtained by least-squares fitting are 72, 199, 996, 3030, 6300 $\mu$M at $C_{salt}$ = 15, 20, 28, 38, 48 mM, respectively. The effect of the actin filament length on $\tilde{K}_d$ was negligible (see the results for the actin trimer and pentamer in Figure 2B). We then compared these $\tilde{K}_d$ values with those measured by an in vitro titration experiment by Katoh and Morita,[16] which is the most carefully controlled and systematically conducted experiment as far as we know. Figure 2B shows that the salt-concentration dependence of the *in silico* $\tilde{K}_d$ is similar to that of the in vitro $\tilde{K}_d$ measured in the presence of ATP. These results ensure that the residue-level coarse-grained model with the Debye−Hückel electrostatics has the ability to capture one of the important characteristics of the actin−myosin binding—the enthalpy-driven binding due to the electrostatic interaction. It is also noteworthy that the *in silico* $\tilde{K}_d$ values are larger than the in vitro ones and that they are more sensitive to the salt concentration than the in vitro ones (see the steeper slope for the *in silico* data). These points will be discussed in detail later.

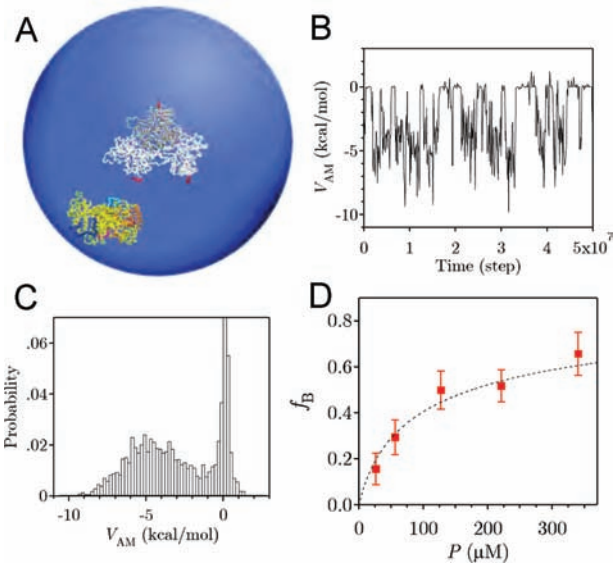


**Figure 1.** *In silico* titration. (A) Encapsulated actin−myosin system used in this study. An actin filament (trimer), located at the center, and myosin (yellow) are confined in a spherical capsule (coloring details for actin and myosin are the same as in Figure 4). In this case, the radius of the sphere is 158 Å, and the concentration of myosin and the actin filament, denoted by $P$, is 128 $\mu$M. (B) Representative trajectory of actin−myosin interaction energy $V_{AM}$ at $P$ = 128 $\mu$M, $T$ = 293 K, and the salt concentration $C_{salt}$ = 20 mM. (C) The probability distribution of the actin−myosin interaction energy resulting from eight independent trajectories conducted at $P$ = 128 $\mu$M, $T$ = 293 K, and $C_{salt}$ = 20 mM. (D) Fractional ratio of the bound state, $f_B$, as a function of $P$ ($T$ = 293 K and $C_{salt}$ = 20 mM). Error bars represent the standard errors (at 95% confidence level) estimated from the multiple (at least five) independent trajectories conducted at each $P$ . By fitting the simulated $f_B$ to eq 5 (dotted line), we obtained the normalized dissociation constants $\tilde{K}_d$ (see Materials and Methods).

**Temperature Dependence of Binding Affinity.** Another important property of the actin−myosin binding is to be seen in the temperature dependence of the binding affinity. The binding affinity is quantified by the binding free-energy $\Delta G^\circ$, which is calculated by $RT \ln(\tilde{K}_d/C^\circ)$ assuming the standard concentration $C^\circ$ of 1 M as usual.[23] Figure 3 shows that the binding affinity is strengthened as temperature is increased. It also shows that the temperature dependence is again in good agreement with that observed in vitro in the presence of ATP.[16] From the slope and the $y$-intercept of the regression line, we can evaluate $\Delta S^\circ$ and $\Delta H^\circ$ (the standard entropy and enthalpy changes upon binding, respectively), by assuming that $\Delta S^\circ$ and $\Delta H^\circ$ are independent of temperature. The resulting $\Delta S^\circ$ is positive (+20 cal/mol/K) and hence indicates that the binding is entropy driven. On the other hand, the resulting $\Delta H^\circ$ is also positive (+1.9 kcal/mol), indicating that the binding is unfavorable in terms of enthalpy and hence cannot be driven


dx.doi.org/10.1021/ja301447j | J. Am. Chem. Soc. 2012, 134, 8918−8925

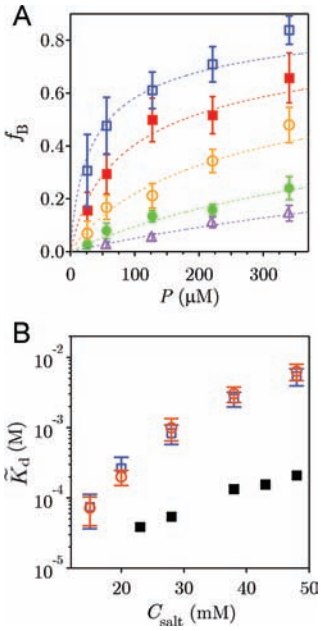


**Figure 2.** Salt-concentration dependence of actin−myosin binding. (A) Titration curves at $C_{salt}$ = 15 mM (open squares), 20 mM (filled squares), 28 mM (open circles), 38 mM (filled circles), and 48 mM (triangles) at 293 K. See the caption of Figure 1D for other details. (B) Salt-concentration dependence of $\tilde{K}_d$. Results for actin trimer (open squares) and pentamer (open circles) are shown. The in vitro data by Katoh and Morita[16] measured in the presence of ATP at 293 K (filled squares) are shown for comparison.

by enthalpy. The positive $\Delta H°$ (together with the positive $\Delta S°$) is in accord with the in vitro experiment[16] where the *entropy*-driven binding was argued, but apparently conflicts with the *enthalpy*-driven binding due to the electrostatic interaction we just mentioned in the previous subsection. We now are faced with the conflict between entropy- and enthalpy-driven binding mechanisms within our own results. (Note that $\Delta S°$ was little affected by the salt concentration, while $\Delta H°$ was decreased at a lower salt concentration, as seen in Figure 3.)

The succinctness of our computational model manifests its power at this point to resolve the above conflict. In our model, because the electrostatic interaction (see eq 1) is the only attractive intermolecular interaction, there is no doubt that the enthalpic contribution due to the electrostatic interaction between actin and myosin drives the binding. Moreover, it is important to note that the electrostatic interaction becomes strengthened as temperature is increased, because we took the temperature-dependent dielectric property of the aqueous environment into account; the dielectric constant decreased with the increase in temperature (from 87.9 at 273 K to 73.2 at 313 K),[24] thus leading to stronger electrostatic interaction at higher temperatures. This temperature enhancement indicates that the electrostatic interaction itself is a free energy with a positive entropic contribution. This positive entropic contribution is related to the temperature-enhanced orientational disorder of water molecules, which is implicitly embedded in the temperature dependence of the dielectric constant. Therefore, a more precise description would be that the enthalpy (due to the electrostatic interaction between actin and myosin) provides the basal binding affinity and the entropy (due to the orientational disorder of water molecules) enhances it at higher temperatures. We also note that the Debye length, another important parameter, is almost unchanged as the temperature is increased because the enhanced electrostatic interaction between counterions and proteins counteracts the enhanced thermal motion of the counterions (see also Materials and Methods).

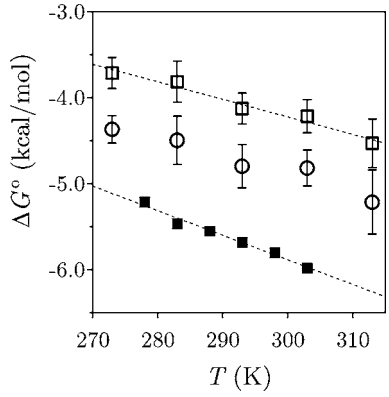


**Figure 3.** Temperature dependence of the binding free energy. The *in silico* data are those obtained at $C_{salt}$ = 28 mM (open squares) and 20 mM (open circles). The in vitro data by Katoh and Morita[16] measured in the presence of ATP at $C_{salt}$ = 28 mM (filled squares) are shown for comparison. The dotted line represents the least-squares line, which gives the *in silico* fitting parameters of $\Delta S°$ = 20 (±2) cal/mol/K and $\Delta H°$ = 1.9 (±0.6) kcal/mol ($C_{salt}$ = 28 mM), while the in vitro fitting parameters are $\Delta S°$ = 29 (±2) cal/mol/K and $\Delta H°$ = 2.7 (±0.6) kcal/mol.

**Actin−Myosin Complex Structure.** We then looked into structural features of the actin−myosin complex observed in our *in silico* experiment. To do this, we conducted cluster analysis against a large number of the low-energy actin−myosin complex structures we obtained and then examined the representative structure for each cluster (see Materials and Methods). In Figure 4, the representative structures for largest clusters are shown. In all structures, myosin loop 2 (blue), which is rich in positively charged residues, is positioned closely to actin subdomain 1, including the N-terminus (red), which is rich in negatively charged residues. Thus, from the structural viewpoint, we can confirm the enthalpy-driven binding due to the electrostatic interaction. Furthermore, it is noteworthy that we can find structures (C2, C3, C5, and C6) that are similar to the complex structure[25−29] of the electron microscopic (EM) models with regard to the position and orientation of myosin relative to the actin filament (see the model structure refined by Lorenz and Holmes[25] added in Figure 4). In these representative structures (C2, C3, and C6), the positively charged loop 3 of myosin (cyan) is found to interact with the subdomain 1 of the adjacent actin on the plus-end side, as has been observed in EM models.[25−28] It is also noteworthy that we can find an unusual structure (C7) in which another positively charged small loop (magenta) interacts with actin, and this unusual mode of actin−myosin interaction has indeed been suggested by an earlier experiment.[30]

The variety of the complex structures we observed, each having substantial statistical importance (see the cluster-size distribution in Figure 4), is consistent with observations by stopped-flow fluorescence and time-resolved EM,[31] and by electron paramagnetic resonance (EPR),[32,33] that myosin is disordered in transient weak-binding. It is also consistent with the finding that the salt concentration and temperature


dx.doi.org/10.1021/ja301447j | J. Am. Chem. Soc. 2012, 134, 8918−8925

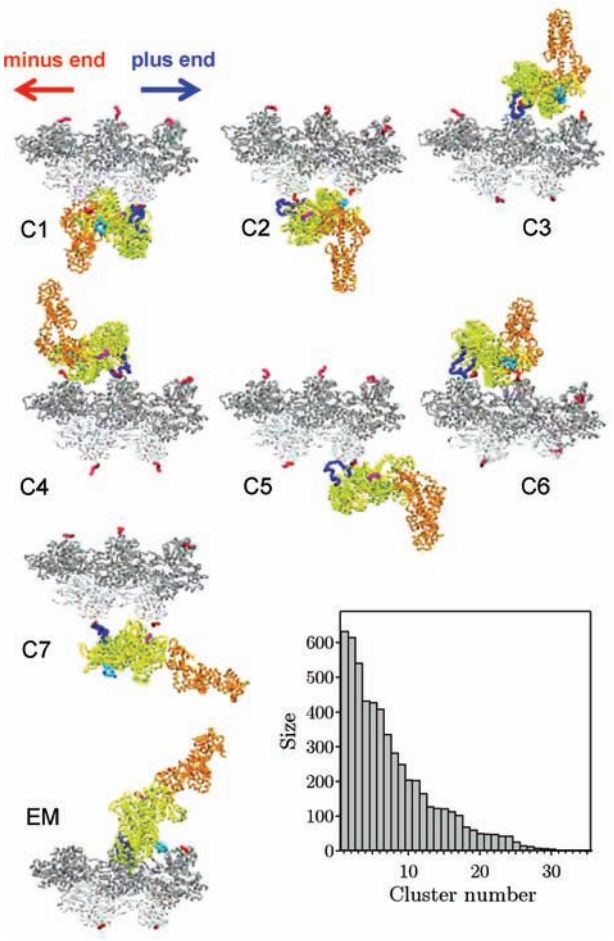


**Figure 4.** Actin−myosin complex structures. Representative structures of the actin−myosin complex for the largest seven clusters (at 293 K and $C_{salt}$ = 20 mM). The *k*th cluster is designated by "C*k*". The lower *k* is, the higher the cluster size, as shown in the bottom-right panel. The cluster size is defined by the number of the structures belonging to the cluster (a total of 5561 structures are grouped into 35 clusters). Filamentous actin (pentamer) is shown in gray (dark and light grays for upper- and lower-strand actin molecules, respectively), with the N-terminus of each molecule (residues 1−4) in red. Myosin is shown in yellow, with the lever-arm domain in orange, loop 2 (residues 621−647) in blue, loop 3 (residues 567−578) in cyan, and the small positively charged loop (residues 144−148) in magenta. The electron microscopic (EM) model refined by Lorenz and Holmes[25] is also shown for comparison.

dependences of $\tilde{K}_d$ we observed showed a good agreement with those observed in vitro in the presence of ATP[16] (ATP brings the actin−myosin complex into the weak binding state[34,35]). These agreements suggest that the residue-level coarse-grained model with Debye−Hückel electrostatics has the capability to describe weak bindings of proteins.

Moreover, the residue-level coarse-grained model with Debye−Hückel electrostatics is likely to have some ability to address the strong actin−myosin binding, because the EM models[25−29] to which a number of observed complex structures showed similarity represent the strong binding complex. Those observed complex structures are thought to be the precursors of the strong-binding complex, guiding myosin into the position and orientation suitable for the subsequent formation of the strong-binding actin−myosin complex. Paying attention to the lever-arm position of myosin (colored in orange in Figure 4), a mere transition from a precursor structure to the strong-binding complex (see, for example, the transition from C3 to EM in Figure 4) can move the lever arm toward the plus end of the actin filament and hence generate mechanical force, as has been suggested by previous studies.[31,36,37] This force-generation mechanism may be involved in the second step of the two-step force-generation mechanism,[38] while the first step is likely to involve the unidirectional thermal hopping (biased Brownian motion) over the weak-binding structures.[18] In addition, the transition from the precursor structures to the strong-binding complex (see again the transition from C3 to EM) can generate torque around the long axis of the actin filament, which is consistent with the rotation of the actin filament observed in an in vitro gliding assay.[39,40]

## ■ DISCUSSION

We have shown that the actin−myosin binding is enthalpy driven due to the attractive electrostatic interaction between actin and myosin. We have also mentioned that the attractive electrostatic interaction includes a positive entropic contribution. Therefore, the net enthalpic change upon actin−myosin binding, which implicitly includes the unfavorable enthalpic change relating to the orientational disorder of water, may become positive. To affirm the sign of $\Delta H^\circ$, it is valuable to consult $\Delta H^\circ$ measured by calorimetry. A recent calorimetric measurement by Takacs et al.[41] has indeed shown that $\Delta H^\circ$ is negative for the binding of squid myosin II to actin, although it is difficult to draw a decisive conclusion from the calorimetric data due to the calorimetric component arising from the rearrangement of the actin filament upon myosin binding and due to the substantial dependence of $\Delta H^\circ$ on the amino acid sequence of myosin. The enthalpy-driven actin−myosin binding is thus supported by the calorimetric measurement.

The temperature-enhanced binding due to electrostatic interaction we have shown implies that electrostatic interaction may appear to be hydrophobic. In the present study, this "pseudo-hydrophobic" interaction is caused by the decrease of the dielectric constant of water with increasing temperature. The dielectric constant is also decreased if the rotational motion of water molecules is somehow restricted. Such situation is likely to occur around a hydrophobic surface; indeed, Despa et al.[42] theoretically indicated that the aqueous dielectric constant is decreased near the hydrophobic surface and suggested that the hydrophobic surface drives intermolecular binding via the enhanced electrostatic interaction as a result of the decrease of the nearby aqueous dielectric constant. This is another interesting situation where the pseudo-hydrophobic interaction may arise.

Regarding temperature-enhanced binding, we also point out that $\Delta S^\circ$ obtained through $K_d$ is affected by the choice of the standard concentration $C^\circ$. This point is likely to be forgotten because $C^\circ$ is almost always taken to be 1 M and is usually omitted, as has been cautioned earlier.[2,7,43] The choice of $C^\circ$ does not matter as far as the difference of $\Delta S^\circ$ is concerned, and the same $C^\circ$ is used so that we can compare the *in silico* and in vitro $\Delta S^\circ$ values, as has been done in this study. However, it is worth remembering that the $\Delta S^\circ$ value itself is affected by $C^\circ$, and the concentration of 1 M is much higher than a typical solution concentration of large macromolecules like proteins (note that 1 M means that the volume per molecule is as small as 1660 Å$^3$, and that a higher $C^\circ$ results in a positive shift of $\Delta S^\circ$).


dx.doi.org/10.1021/ja301447j | *J. Am. Chem. Soc.* 2012, 134, 8918−8925

In addition to the good agreement in salt-concentration and temperature dependences of the observed binding affinity with the in vitro experiment,[16] we have pointed out that the binding affinity was weaker than the in vitro one and that the salt-concentration dependence was stronger than that observed in the experiment. The latter is consistent with the fact that ionizable residues (except for histidine) were fully charged in our study (see Materials and Methods), whereas they are not in reality. By comparing the slopes in the log $\tilde{K}_d$ vs $C_{salt}^{1/2}$ plot (Figure 5) that reflect the product of the net effective charges of

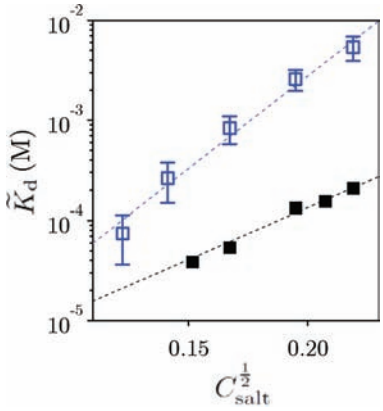


**Figure 5.** Estimation of the ionization rate. The dissociation constants ($\tilde{K}_d$) are plotted as a function of the square root of the salt concentration ($C_{salt}^{1/2}$). The *in silico* data (open blue squares) and the in vitro data[16] (filled squares) are shown, together with their regression lines (dotted lines), respectively. Note that the slope of the regression line is approximately proportional to the product of the net effective charges of myosin and actin.[44]

the two interacting molecules[44] (generally known as the "Debye–Hückel limiting law"), we can estimate that the actual ionization rate is about 0.75 on average (assuming the same average ionization rates for both actin and myosin). Regarding the former (the underestimation of the binding affinity), one of the causes may be due to molecular flexibility. For example, flexibility of surface loops would affect the binding affinity, as has been shown in the previous study,[18] and thus we modeled this with care in the present study by employing a multiscale approach (see eq 3 in Materials and Methods). On the other hand, flexibility resulting from the side chain's degrees of freedom was omitted in the present coarse-grained model. Considering this and placing charges on the side-chain positions (instead of on the main-chain positions) would facilitate the electrostatic interaction and strengthen the binding affinity. Structural plasticity that allows large-scale structural changes would also affect the binding affinity; indeed, large-scale open-close motion of the actin-binding cleft of myosin is thought to regulate the actin–myosin binding affinity.[26,28,29,41,45] Although the structural plasticity was partly incorporated in the present model by employing the so-called Gō-like model,[46–48] an extended model[49,50] that facilitates such a large-scale motion as in the actin-binding cleft and also in the actin filament might improve the underestimation of the binding affinity.

It is obvious that a more crucial cause of the underestimation comes from the intermolecular interaction. First, although we used the dielectric constant of bulk water[24] for the Debye–Hückel parameter $\varepsilon_r$, there is a possibility that $\varepsilon_r$ is effectively smaller than that of the bulk water (cf. the above-mentioned reduced dielectric constant near the hydrophobic surface[42]). We thus examined how the binding affinity is affected by $\varepsilon_r$. Interestingly, the binding affinity was increased with decreasing $\varepsilon_r$ as shown in Figure 6, approaching the in vitro $\tilde{K}_d$ value at $\varepsilon_r$

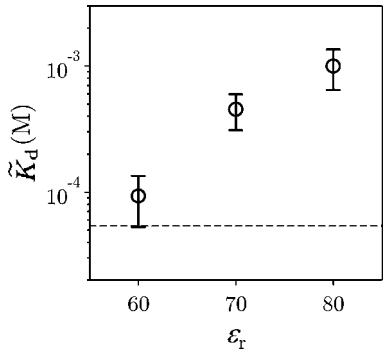


**Figure 6.** Influence of the dielectric constant on the dissociation constants. By conducting the *in silico* titration using lower dielectric constants ($\varepsilon_r$ = 60 and 70), we obtained the dielectric constant dependence of $\tilde{K}_d$ (at 293 K and $C_{salt}$ = 28 mM). The broken line indicates the in vitro value.[16].

= 50–60. This result indicates the importance of the spatial inhomogeneity of the dielectric constant, in addition to its temperature dependence. Second, the hydrophobic interaction, which should also strengthen the binding affinity, was omitted in this study to clarify the role of the electrostatic interaction. To fully examine the effect of the hydrophobic interaction, it is important to take into account the particle effect of solvent water molecules, as has been shown in the recently developed molecular theory.[12,17] Such a full examination, however, is beyond the scope of the present study, so that we briefly assessed the contribution of the hydrophobic interaction by employing the knowledge-based statistical potential by Kim and Hummer[19,20] that can effectively account for the hydrophobic interaction. As is clearly seen in Figure 7, the binding affinity was increased and came to agree well with the in vitro $\tilde{K}_d$

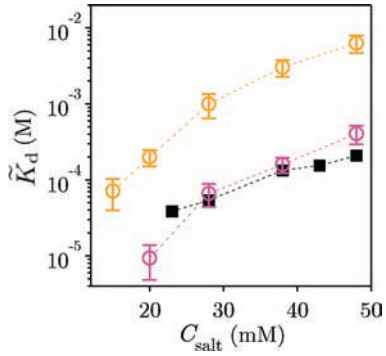


**Figure 7.** Influence of the hydrophobic interaction on the dissociation constants. To briefly examine the effect of the intermolecular hydrophobic interaction, we used the same potential functions and accompanying parameters as proposed by Kim and Hummer[19] (i.e., eqs 2 and 3 in ref 19. and the adjusted Miyazawa–Jernigan parameters[51]) in place of the simple repulsive interaction (eq 2 in Materials and Methods). The salt-concentration dependence of $\tilde{K}_d$ at 293 K obtained when the hydrophobic interaction was taken into account is shown (magenta circles). For comparison, the data for the simple repulsive interaction (orange circles) and the in vitro data[16] (filled squares) are also presented.


dx.doi.org/10.1021/ja301447j | J. Am. Chem. Soc. 2012, 134, 8918–8925

values, suggesting the potentially important contribution of the hydrophobic interaction (particularly for the strong binding).

If all of the binding-affinity-enhancing factors mentioned above were taken into account, the binding affinity would become too strong; i.e. the underestimation would turn into overestimation. However, the overestimation is rather reasonable because it can be counterbalanced by the last component to be considered: the Born energy (i.e., electrostatic self-energy). The Born energy is always positive and inversely proportional to the dielectric constant, $\varepsilon$, of the environment. Therefore, for charged residues on the binding surface, the Born energy change upon binding is energetically unfavorable, since those residues experience a dielectric environmental change from $\varepsilon_{aq}$ to $\varepsilon_{non\text{-}aq}$ ($\varepsilon_{aq} > \varepsilon_{non\text{-}aq}$). As far as weak binding is concerned, as is the case in this study, the contribution of the Born energy change would not be so large because protein molecules remain substantially solvated in the weak-binding state. On the other hand, it would become large for the strong binding where the desolvation is completed. Thus, the temperature-enhanced binding due to electrostatics may arise for the strong binding through the Born energy; the decrease of $\varepsilon_{aq}$ with increasing temperature makes the Born energy change less unfavorable and hence strengthens the binding affinity at higher temperatures. The pseudo-hydrophobic interaction could arise not only from the electrostatic interaction but also from the electrostatic self-energy.

## CONCLUSION

In summary, we showed that the coarse-grained model with the Debye–Hückel electrostatics, in which temperature dependence of the dielectric constant is taken into account, explains how thermodynamically different binding mechanisms can coexist, reinforcing the fundamental importance of the electrostatics in the protein–protein interaction. Furthermore, we argued the possibility that the electrostatic interaction may appear to be hydrophobic. From the structural (as well as thermodynamic) viewpoint, the potential capability of the coarse-grained model in describing protein–protein binding, particularly transient weak-bindings, was confirmed. While further studies are necessary to improve the coarse-grained models, the results of the present study give us hope that the coarse-grained models with proper electrostatics will be highly useful in studying the association–dissociation dynamics of more complicated and larger macromolecular systems as in a cell.

## MATERIALS AND METHODS

**Structures Used for Myosin and Actin.** For myosin, the X-ray crystal structure of chicken skeletal myosin (PDB ID: 2mys)[52] was used. The actin-binding cleft of this myosin structure is in the open state, so that this structure is presumed to be in the weak binding state.[26,29] Missing residues were complemented by using the homology modeling program MODELLER.[53] For actin, we used the filament structure that was recently refined.[54]

**Coarse-Grained Model.** Each amino acid of myosin and actin was coarse-grained as one bead, just like typical coarse-grained models employed in the theoretical studies of protein folding,[46−48] functional,[49,50] and binding dynamics.[18−22] For the actin–myosin intermolecular interactions, only two interactions were considered for simplicity. One is the Debye–Hückel type electrostatic interaction as used in the previous studies,[18−22] which considers ionic screening of the electrostatic interaction such that

$$V_{AM}^{ele} = \sum_{i,j} q_i q_j \exp\left(-r_{ij}/\lambda_D\right)\Big/ 4\pi\varepsilon_0\varepsilon_r r_{ij} \quad (1)$$

where $r_{ij}$ is distance between the residues $i$ and $j$, $q_i$ is the charge of residue $i$ ($-e$ for Asp and Glu, $+e$ for Lys and Arg, $+0.5e$ for His, and 0 for others; $e$ represents the elementary charge), and $\lambda_D$ is the Debye length given by $(\varepsilon_r\varepsilon_0 k_B T/2e^2 N_A C_{salt})^{1/2}$ ($\varepsilon_r$ and $\varepsilon_0$: relative and vacuum dielectric constants, $T$: temperature, $k_B$: Boltzmann constant, $C_{salt}$: salt (1:1 salt) concentration, $N_A$: Avogadro's number). Importantly, we considered the temperature-dependence of the dielectric constant of the aqueous environment,[24] so that $\varepsilon_r$ was decreased with increasing $T$ ($\varepsilon_r$ = 87.9, 85.9, 84.0, 82.1, 80.2, 78.4, 76.6, 74.9, 73.2 at $T$ = 273, 278, 283, 288, 293, 298, 303, 308, 313 K, respectively), while $\lambda_D$ remained almost unchanged because of the counterbalance between $\varepsilon_r$ and $T$. The other intermolecular interaction employed in the present study is the short-range repulsive interaction given by

$$V_{AM}^{rep} = \sum_{i,j} u_{rep}(\sigma_{rep}/r_{ij})^{12} \quad (2)$$

where $\sigma_{rep}$ = 5.9 Å and $u_{rep}$ = 0.43 kcal/mol, which gives almost the same functional shape as that used in the previous study.[18] $\sigma_{rep}$ was set to the average van der Waals diameter of amino acids.[19] For the intramolecular interactions, the Gō potential[46,47] was used except for the flexible regions near the molecular surfaces: loops 1–4 and cardiomyopathy loop of myosin and the N-terminus of actin. These flexible regions were modeled by a multiscale approach; the parameters for the coarse-grained potential for the angle formed by the three consecutive residues were derived from the potential of mean force (PMF) obtained from the all-atom simulation of myosin. The obtained PMF showed a double-well profile (each well corresponding to helix and extended conformations) and was fitted by a double-well function as in the previous study[49,50] such that

$$V_{ang}(\theta) = (V_{ang}^{\alpha}(\theta) + V_{ang}^{\beta}(\theta))/2 - ((V_{ang}^{\alpha}(\theta) - V_{ang}^{\beta}(\theta))/2 + \Delta)^{1/2} \quad (3)$$

where $V_{ang}^{a}(\theta) = 126 \times (\theta - 1.5)^2$, $V_{ang}^{b}(\theta) = 8.9 \times (\theta - 2.4)^2$ and $\Delta = 7.2$ (angles are in radians, and energies are in kcal/mol). For the flexible regions, only this angle potential and the bond potential[46,47] to maintain chain connectivity were used.

***In silico* Titration.** Unlike the previous study[18] where myosin was restricted to move along the actin filament, in the present study myosin was allowed to move freely within a spherical capsule. The mass center of the actin filament was placed at the center of the sphere and was immobilized. To confine myosin within the sphere, a half-harmonic restoring potential was applied to the mass center of myosin such that

$$V_{cap} = \begin{cases} k_{cap}(R - R_{cap})^2 & (R > R_{cap}) \\ 0 & (R \le R_{cap}) \end{cases} \quad (4)$$

where $R_{cap}$ is the radius of the sphere, $R$ is the radial distance of the mass center of myosin from the center of the sphere, and $k_{cap}$ = 500 kcal/mol/Å$^2$ (we set $k_{cap}$ at this rather large value to strictly confine the mass center of myosin within the capsule). Thus, the concentration of myosin and the actin filament, $P$, is approximately given by $P = 1/(4\pi R_{cap}^3/3 - V_{ex})N_A^{-1} \times 10^{33}$ ($\mu$M), where $V_{ex}$ represents the inaccessible (excluded) volume due to the finite volume of proteins ($3.5 \times 10^6$ and $5.0 \times 10^6$ Å$^3$ for actin trimer and pentamer systems, respectively). The fractional ratio of the actin–myosin-bound state, $f_B$, as a function of $P$ is given by[55]

$$f_B(P) = (2P + K_d - (K_d^2 + 4K_d P)^{1/2})/2P \quad (5)$$

where $K_d$ is the dissociation constant. In this study, we calculated $f_B$ by conducting multiple (5–44) molecular dynamics simulations ($5 \times 10^7$ steps) using low-viscosity Langevin dynamics to control temperature and to enhance structural sampling. All simulations were performed


dx.doi.org/10.1021/ja301447j | J. Am. Chem. Soc. 2012, 134, 8918–8925

using CafeMol[56] with some modifications. By changing $R_{cap}$ (and accordingly $P$), we obtained titration curves and corresponding $K_d$ values by fitting the simulated $f_B$ to the above formula. Assuming that an actin filament with $n$ monomers has $n$-fold higher affinity than a single actin monomer, we multiplied $K_d$ by $n$ to obtain the normalized (i.e., per actin monomer) dissociation constants $\tilde{K}_d$.

**Clustering of the Actin−Myosin Complex Structures.** For every pair of the low-energy (lowest 10%) actin−myosin complex structures obtained in our simulation (5561 structures), the structural distance was calculated using root-mean-square deviation (rmsd) between the myosin structures, which can discriminate the positions and orientations of myosin relative to the actin filament. According to this distance, neighboring myosin structures were grouped into a cluster in a hierarchical manner. The intercluster distance was calculated using the group average method. We used the clusters obtained at the intercluster distance threshold of 50 Å. Thus, the low-energy structures were grouped into 35 clusters. The largest clusters (i.e., clusters with largest populations) were analyzed in detail. To select the representative structure in each cluster, we calculated the structure packing number[57] for the structure $i_k$ in a cluster $k$, which is defined as $\zeta_k(i_k) = \sum_{j_k} \exp(-(d_{i_k j_k}/\sigma)$, where $d_{i_k j_k}$ is the distance between the structures $i_k$ and $j_k$ in the cluster $k$, and $\sigma$ was set at 10 Å. $\zeta_k(i_k)$ indicates how many structures are close to the structure $i_k$, and the structure with the highest $\zeta_k$ value was selected as the representative structure of the cluster $k$.

## AUTHOR INFORMATION


### Corresponding Author

mtkn@waseda.jp


### Notes

The authors declare no competing financial interest.

## ACKNOWLEDGMENTS

We thank Masahiro Kinoshita for initiating discussion, Masaki Sasai and Tomoki Terada for continuous discussion, and Yoshimi Fujitsuka for providing the clustering program. This work was partially supported by Grants-in-Aids for Scientific Research on Innovative Areas from MEXT. K.O. is supported by Research Fellowships of the Japan Society for the Promotion of Science for Young Scientists. The computations were partly performed using the Research Center for Computational Science, Okazaki, Japan.

## REFERENCES


(1) Alberts, B.; Johnson, A.; Lewis, J.; Raff, M.; Roberts, K.; Walter, P. *Mol. Biol. Cell*, 5th ed.; Garland Science: New York, 2007.
(2) Gilson, M. K.; Given, J. A.; Bush, B. L.; McCammon, J. A. *Biophys. J.* **1997**, *72*, 1047−1069.
(3) Doty, P.; Myers, G. E. *Discuss. Faraday Soc* **1953**, *13*, 51−58.
(4) Kauzmann, W. *Adv. Protein Chem.* **1959**, *14*, 1−63.
(5) Steinberg, I. Z.; Scheraga, H. A. *J. Biol. Chem.* **1963**, *238*, 172−181.
(6) Chothia, C.; Janin, J. *Nature* **1975**, *256*, 705−708.
(7) Finkelstein, A. V.; Janin, J. *Protein Eng.* **1989**, *3*, 1−3.
(8) Tidor, B.; Karplus, M. *J. Mol. Biol.* **1994**, *238*, 405−414.
(9) Karplus, M.; Janin, J. *Protein Eng.* **1999**, *12*, 185−186.
(10) Pratt, L. R. *Annu. Rev. Phys. Chem.* **2002**, *53*, 409−436.
(11) Chandler, D. *Nature* **2005**, *437*, 640−647.
(12) Kinoshita, M. *Front. Biosci.* **2009**, *14*, 3419−3454.
(13) Ball, P. *Chem. Rev.* **2008**, *108*, 74−108.
(14) Tonomura, Y.; Tokura, S.; Sekiya, K. *J. Biol. Chem.* **1962**, *237*, 1074−1081.
(15) Highsmith, S. *Arch. Biochem. Biophys.* **1977**, *180*, 404−408.
(16) Katoh, T.; Morita, F. *J. Biochem.* **1996**, *120*, 189−192.
(17) Amano, K.; Yoshidome, T.; Iwaki, M.; Suzuki, M.; Kinoshita, M. *J. Chem. Phys.* **2010**, *133*, 045103.
(18) Takano, M.; Terada, T. P.; Sasai, M. *Proc. Natl. Acad. Sci. U.S.A.* **2010**, *107*, 7769−7774.
(19) Kim, Y. C.; Hummer, G. *J. Mol. Biol.* **2008**, *375*, 1416−1433.
(20) Kim, Y. C.; Tang, C.; Clore, G. M.; Hummer, G. *Proc. Natl. Acad. Sci. U.S.A.* **2008**, *105*, 12855−12860.
(21) Hyeon, C.; Onuchic, J. N. *Proc. Natl. Acad. Sci. U.S.A.* **2007**, *104*, 17382−17387.
(22) Hyeon, C.; Onuchic, J. N. *Biophys. J.* **2011**, *101*, 2749−2759.
(23) McQuarrie, D. A.; Simon, J. D. *Physical Chemistry: A Molecular Approach*; University Science Books: Sausalito, 1997.
(24) Archer, D. G.; Wang, P. *J. Phys. Chem. Ref. Data* **1990**, *19*, 371−411.
(25) Lorenz, M.; Holmes, K. C. *Proc. Natl. Acad. Sci. U.S.A.* **2010**, *107*, 12529−12534.
(26) Rayment, I.; Rypniewski, W. R.; Schmidt-Base, K.; Smith, R.; Tomchick, D. R.; Benning, M. M.; Winkelmann, D. A.; Wesenberg, G.; Holden, H. M. *Science* **1993**, *261*, 50−58.
(27) Milligan, R. A. *Proc. Natl. Acad. Sci. U.S.A.* **1996**, *93*, 21−26.
(28) Mendelson, R.; Morris, E. P. *Proc. Natl. Acad. Sci. U.S.A.* **1997**, *94*, 8533−8538.
(29) Holmes, K. C.; Angert, I.; Kull, F. J.; Jahn, W.; Schröder, R. R. *Nature* **2003**, *425*, 423−427.
(30) Dan-Goor, M.; Muhlrad, A. *Biochemistry* **1991**, *30*, 400−405.
(31) Walker, M.; Zhang, X.-Z.; Jiang, W.; Trinick, J.; White, H. D. *Proc. Natl. Acad. Sci. U.S.A.* **1999**, *96*, 465−470.
(32) Thomas, D. D.; Ramachandran, S.; Roopnarine, O.; Hayden, D. W.; Ostap, E. M. *Biophys. J.* **1995**, *68*, 135S−141S.
(33) Thompson, A. R.; Naber, N.; Wilson, C.; Cooke, R.; Thomas, D. D. *Biophys. J.* **2008**, *95*, 5238−5246.
(34) Lymn, R. W.; Taylor, E. W. *Biochemistry* **1971**, *10*, 4617−4624.
(35) Geeves, M. A.; Holmes, K. C. *Annu. Rev. Biochem.* **1999**, *68*, 687−728.
(36) Berger, C. L.; Thomas, D. D. *Biophys. J.* **1994**, *67*, 250−261.
(37) Kodera, N.; Yamamoto, D.; Ishikawa, R.; Ando, T. *Nature* **2010**, *468*, 72−76.
(38) Taylor, K. A.; Schmitz, H.; Reedy, M. C.; Goldman, Y. E.; Franzini-Armstrong, C.; Sasaki, H.; Tregear, R. T.; Poole, K.; Lucaveche, C.; Edwards, R. J.; Chen, L. F.; Winkler, H.; Reedy, M. K. *Cell* **1999**, *99*, 421−431.
(39) Nishizaka, T.; Yagi, T.; Tanaka, Y.; Ishiwata, S. *Nature* **1993**, *361*, 269−271.
(40) Beausang, J. F.; Schroeder, H. W., 3rd; Nelson, P. C.; Goldman, Y. E. *Biophys. J.* **2008**, *95*, 5820−5831.
(41) Takács, B.; O'Neall-Hennessey, E.; Hetényi, C.; Kardos, J.; Szent-Györgyi, A. G.; Kovács, M. *FASEB J.* **2011**, *25*, 111−121.
(42) Despa, F.; Fernández, A.; Berry, R. S. *Phys. Rev. Lett.* **2004**, *93*, 228104.
(43) Swanson, J. M. J.; Henchman, R. H.; McCammon, J. A. *Biophys. J.* **2004**, *86*, 67−74.
(44) Highsmith, S. *Biochemistry* **1990**, *29*, 10690−10694.
(45) Klein, J. C.; Burr, A. R.; Svensson, B.; Kennedy, D. J.; Allingham, J.; Titus, M. A.; Rayment, I.; Thomas, D. D. *Proc. Natl. Acad. Sci. U.S.A.* **2008**, *105*, 12867−12872.
(46) Clementi, C.; Nymeyer, H.; Onuchic, J. N. *J. Mol. Biol.* **2000**, *298*, 937−953.
(47) Koga, N.; Takada, S. *J. Mol. Biol.* **2001**, *313*, 171−180.
(48) Onuchic, J. N.; Wolynes, P. G. *Curr. Opin. Struct. Biol.* **2004**, *14*, 70−75.
(49) Okazaki, K.; Koga, N.; Takada, S.; Onuchic, J. N.; Wolynes, P. G. *Proc. Natl. Acad. Sci. U.S.A.* **2006**, *103*, 11844−11849.
(50) Okazaki, K.; Takada, S. *Proc. Natl. Acad. Sci. U.S.A.* **2008**, *105*, 11182−11187.
(51) Miyazawa, S.; Jernigan, R. L. *J. Mol. Biol.* **1996**, *256*, 623−644.
(52) Rayment, I.; Holden, H. M.; Whittaker, M.; Yohn, C. B.; Lorenz, M.; Holmes, K. C.; Milligan, R. A. *Science* **1993**, *261*, 58−65.
(53) Martí-Renom, M. A.; Stuart, A. C.; Fiser, A.; Sánchez, R.; Melo, F.; Šali, A. *Annu. Rev. Biophys. Biomol. Struct.* **2000**, *29*, 291−325.
(54) Oda, T.; Iwasa, M.; Aihara, T.; Maeda, Y.; Narita, A. *Nature* **2009**, *457*, 441−445.

(55) Geeves, M. A.; Jeffries, T. E. *Biochem. J.* **1988**, *256*, 41−46.
(56) Kenzaki, H.; Koga, N.; Hori, N.; Kanada, R.; Li, W.; Okazaki, K.; Yao, X.-Q.; Takada, S. *J. Chem. Theory Comput.* **2011**, *7*, 1979−1989.
(57) Betancourt, M. R.; Skolnick, J. *J. Comput. Chem.* **2001**, *22*, 339−353.

## ■ NOTE ADDED AFTER ASAP PUBLICATION

This paper was published ASAP on May 15, 2012. A typographical error in the equation describing the concentration of myosin and the actin filament, P, following equation 4, has been corrected. The revised version was posted on May 21, 2012.